Effective Data-driven multi-criteria optimization of black-box processes: a case study of PBF-LB/M of a magnesium alloy

Andrzej Pawlak[a], **Yunsheng Tian**[b], **Wojciech Matusik**[b],

[a] Faculty of Mechanical Engineering, Wroclaw University of Science and Technology, Lukasiewicza 5, 50-371, Wroclaw, Poland
[b] Computer Science and Artificial Intelligence Laboratory, Massachusetts Institute of Technology, 32 Vassar St, Cambridge MA 02139, USA

Corresponding author: andrzej.p.pawlak@pwr.edu.pl

Abstract

Optimizing complex processes influenced by multiple variables is time-consuming and labor-intensive. A single optimal solution for one criterion often fails when the evaluation criterion changes, necessitating further optimizations. Multi-criteria optimization using Pareto fronts identifies regions in the design space that balance conflicting objectives. Machine learning-based approaches enable rapid process response recognition, even without prior domain knowledge, providing a strong foundation for targeted optimization.

This study evaluates the effectiveness of multi-criteria optimization in black-box processes, exemplified by the PBF-LB/M process for a magnesium alloy. The optimization criteria taken into account in our study were mutually exclusive process efficiency expressed by sample relative density and process efficiency, as well as material quality determined by its hardness.

Using the full range of four key process parameters, we applied Latin Hypercube Sampling (LHS) to select 18 initial parameter sets. Subsequent iterations employed the Noisy Expected Hypervolume Improvement (qNEHVI) method, testing ten additional batches of 20 parameter sets each. Just by the fourth optimization iteration, we achieved a significant hypervolume increase and determined a Pareto front.

The results demonstrate that combining data-driven multi-criteria optimization with surrogate models significantly accelerates process optimization while reducing experimental costs. This approach not only enhances efficiency but also provides deeper insights into process behaviour, offering a versatile framework adaptable to various industrial applications. By shifting away from conventional design of experiments (DoE), this method unlocks new possibilities for optimizing complex manufacturing processes with minimal trial-and-error.

Keywords

Bayesian optimization, Expected Hypervolume Improvement, Additive Manufacturing, PBF-LB, Porosity,

Introduction

Traditional ways of optimizing additive processes, especially such complex ones as Laser Based Powder Bed Fusion of Metals (PBF-LB/M), are a multi-step process [1, 2]. Given the large number of process parameters that directly influence the result, optimization is typically performed in a sequential manner, where each stage builds upon the optimal values determined in previous steps. In a traditional trial and error method, first, single scanning tracks are optimized on a one-dimensional scale, assessing the quality of the obtained material melting [3–5]. In the next step, further parameters are taken into account in the production of

3-dimensional samples [6], in order to finally determine the values of the last parameters affecting the surface quality of the printed objects [7]. The presented approach is very time-consuming and requires many experiments, and concerns only the quality of the processed material and product, not taking into account the efficiency of the process, which directly affects the cost of the manufactured objects. This approach also consumes substantial materials to produce experimental samples that do not necessarily contribute to achieving the optimization goal. In addition, once the values of some parameters are set at the initial stages, they remain constant at subsequent stages, downplaying their interactions with the parameters analyzed in subsequent stages. Some researchers, based on literature data, suggest further experiments to optimize processes, arbitrarily setting the values of the changed parameters, following the principle of maintaining a constant density of energy supplied to the melted material [8].

A more analytical approach to process optimization PBF-LB uses Design of Experiments (DoE) tools. This approach saves time, raw materials and more effectively evaluates the impact of several variable parameters at the same time, also taking into account the interactions between them [9, 10].

Currently, many researchers are focussing on evaluating new methods of process optimization using Machine Learning (ML) tools, including multi-criteria optimization. Literature sources provide results of the use of Bayesian optimization (BO) tools together with Neural Network (NN), supporting optimization processes by predicting new variants and their performance, from which a sample is then selected for experimental validation [11]. This is driven by the strong connection between process-structure-property of additively processed materials, which is a challenge in PBF-LB/M [12]. The use of Multi-objective Bayesian Optimization (MOBO) algorithms, reported so far, is used both to simulate the processes of laser remelting of metals in terms of temperature and cooling rate on the obtained microstructure of titanium alloys [12], as well as in the optimization of the process in terms of the obtained quality of the material [13], surface quality [14] and mechanical properties such as tensile strength [15], plasticity [16], or fatigue strength [17]. Another work reports the application of Diversity-guided efficient multi-objective optimization (DGEMO), for optimization 316L steel PBF-LB/M process, albeit requiring a large pre-existing dataset [18]. More sophisticated approach was reported by Song, et al. where Multi objective genetic algorithm (MOGA) was applied in the final optimization stage of enhancing material magnetic property, while still the initial optimization of process result in case of basic relative density was made with DoE approach [19]. Khalil et al. [20] used BO to determine the effect of simulated porosity distribution in 17-4PH alloy samples and the process parameters used to produce these samples on the mechanical properties of the material . However, the behaviour of the material was difficult to understand due to the low porosity detection threshold of the CT method used. Furthermore, regardless of the use of ML tools in the optimization of PBF-LB/M processes, the use of machine learning is developed in the areas of process quality control, mainly through their implementation *in situ* process monitoring [21].

Multi-criteria Bayesian optimization tools are also used in the optimization of other additive processes, not only PBF-LB/M but also Directed Energy Deposition (DED) [22]. The significance of ML-driven optimization in additive processes has gained widespread recognition, with some researchers [23] advocating for an open platform to spread knowledge, harmonise approaches and improve understanding of the optimizations performed.

The aim of this study is to evaluate the effectiveness of the application of the new method in the optimization of the PBF-LB/M process, using the algorithm of MOBO. The research is a verification of the application of ML methods for the optimization of AM processes, in which two self-exclusive optimization criteria were used at once: material quality, defined by relative density, and process productivity.

Material and methods

1. Powder Bed Fusion of AZ31 alloy

The optimization of PBF-LB/M process was investigated in this study. All experiments were conducted under argon atmosphere on ReaLizer SLM50 machine (ReaLizer, Borchen, Germany), equipped with a fibre laser of a max power of 100 W focused to d=100 µm spotsize.

The AZ31B magnesium alloy powder was used in this study. Magnesium based alloys are challenging materials for processing, because of its high flammability in oxygen atmosphere and tight processing temperature range between melting and boiling point. While the closed PBF-LB process chamber filled with an inert gas atmosphere reduces the risk of ignition, then the inefficient and limited gas filtration, leads to a problem of dealing the fumes of an evaporation products.

The AZ31B alloy spherical powder (TLS Technik GmbH & Co. Spezialpulver KG, Bitterfeld-Wolfen, Germany) with a particle size distribution of 40-100 µm was used. The powder fraction was initially checked by laser diffractometer HELOS H3776, RODOS T4, R4 (Sympatec GmbH, Clausthal-Zellerfeld, Germany). The powder morphology was also evaluated with the EVO MA25 Scanning Electron Microscope (CARL ZEISS, Oberkochen, Germany) - Fig. 1. The thickness of the deposited powder layers (l_t) was fixed for all experiments to 50 µm.

All samples manufactured for porosity assessment have a cuboid shape of 5x3x5 mm (xyz) size. Samples were built up on a 3 mm thick AZ31 sheet metal plate, without its preheating during the process.

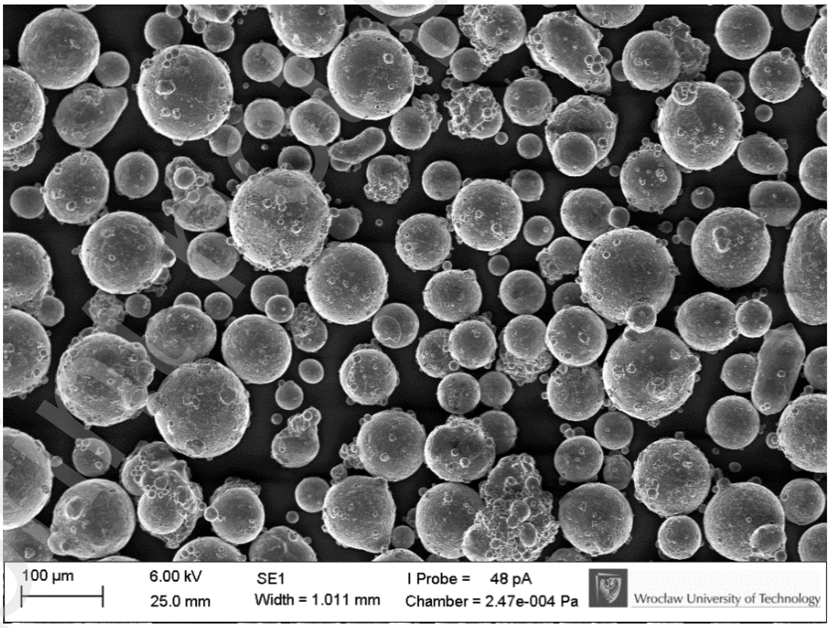

Fig. 1 SEM image of AZ31 powder material used in the study.

2. Optimization problem Set up

Design space

Four processing parameters were selected as input variables: Laser power, laser exposure time, distance between scanning points, and distance between scanning tracks – Table 1.

Selected parameters are commonly known to have the greatest influence on PBF-LB/M process results [24]. All chosen input variables parameters are a constituents of another descriptive PBF-LB/M process parameter – Volume Energy Density (VED) (Eq. 1) [5], which many researchers used as a main input variable, which results the material quality.

$$VED = \frac{P}{V \cdot d \cdot l_t}, [\frac{J}{mm^3}] \quad \textit{Equation 1}$$

VED is calculated as the delivered energy, from P – laser power, per time unit (taken from scanning speed – V) into the processed powder volume. Scanning velocity, in the equipment used in our study is not defined directly, but as a quotient of two other constituent processing parameters distance between scanning points (p_{dist}), and laser exposure time (t_{expo}) (Eq. 2).

$$V = \frac{p_{dist}}{t_{expo}}, [\frac{mm}{s}] \quad \textit{Equation 2}$$

Given the assumption that no prior knowledge of optimal process conditions exists for the processed material, the initial range of each input variable should ideally remain unrestricted, constrained only by hardware limitations. However, we decided to introduce some limitations. First is to make the design variable space discrete and define step size for each parameter. The laser power is defined by the current value, which could be adjusted with every 1 mA, which corresponds to 0.02 W, but in the presented research this variable will take values from the entire possible range with an accuracy of 5 W. Other input variables step size are listed in Table 1. Additionally, further parameter ranges were narrowed. The distance of less than 50 µm between the scanning points and the lines will lead to high overlap, and in turn the higher distance than 100 µm theoretically will lead to no overlap and as a result to increased porosity, or the impossibility of getting solid material. Using very high scanning speeds during melting leads to very thin weld seams, and then again, the line distance even lower than 100 µm could also lead to 0 overlap. Finally, the laser exposure time in single point was limited to a half of maximum possible value. Even with the introduced limitations in possible values of each input variable, the complete number of possible experiments reaches 50.000.

Table 1 The list of input variables, their possible values ranges, limited to the scope studied in this paper, and the size of the value change step.

Process Parameter		**Available range**	**Range**	**Step size**
P	Laser power [W]	0.02-100	5-100	5 W
p_{dist}	Distance between scanning points [µm]	1-1000	50-150	10 µm
t_{expo}	Laser exposure time [µs]	20-1000	20-500	20 µs
h_{dist}	Distance between scanned tracks [µm]	1-1000	50-150	10 µm

Optimization Criteria

Three optimization criteria were selected to be optimized at the same time (Table 2): Relative density (z_1), which determines processed material quality, Process Build rate (z_2) corresponds to the process effectiveness, and Material hardness (z_3), which is a first mechanical property that allows us to compare process results to reference materials. The first and the third objective functions were modelled in the optimization problem with a Gaussian Process, while the Build rate objective is deterministic.

Table 2 The List of criteria for evaluating the effects of the process and their goal in optimization.

Optimization criteria		**Max/min**
z_1	Relative density [%]	Maximize

z_2	Build rate [mm³/s]	Maximize
z_3	Hardness [HV0.1]	Minimize deviation from 55

First of the selected evaluation criteria is main factor for every initial PBF-LB/M process optimization – Relative density. Porosity in the material lead to its discontinuity, so it is the most undesirable material void, which should be eliminated at first, and that the aim in this optimization is to maximize criteria of relative density.

The second optimization criteria stands in the opposite to the first one. To make processes cheaper and widely applicable, because of the high investment in to the PBF-LB/M equipment, the build rate [25](Eq. 3) defined as a product of layer thickness (l_t), hatch distance (h_{dist}) and scan speed (V), should be as high as possible. Productivity is calculated from the processing parameter values and does not have to be measured after the experiment.

$$Build\ rate = l_t \cdot h_{dist} \cdot V \left[\frac{mm^3}{s}\right], \qquad \text{Equation 3}$$

For the magnesium alloy, there is another crucial reason for increasing the process productivity which is the material evaporation. The soot that is produced during material melting limits the maximum processing time, and its deposition inside the machine chamber limits the effectiveness of the optical system. The higher the energy input, which is a result of, e.g. high laser power but also low scanning speed, the more material evaporation and soot in the processing chamber.

The third optimization criteria determines the basic mechanical property. Hardness of a material affects the ductility of the material. The higher the hardness, the more brittle and strong the material the harder to cut/machine it. Laser additive manufacturing processes, as well as welding, heat up the material very quickly, which then cools quickly, leading to an increase in residual stress in the material (very rapid thermal expansion and shrinkage), which increases the hardness. In order to obtain 3D printed metal with mechanical properties comparable to conventional processing techniques, it is necessary to apply additional heat treatment post-process, which leads to a reduction in material stress, a reduction in material hardness and restoration of material ductility. An increase in residual stress in the fabricated material is also a threat to the manufacturing process, as it can lead to bending of the part/sample during the process and collision with the recoating system, or at least distortion of the fabricated part [26]. For aim of the optimization is to achieve material hardness as compared to the reference material set to – 55 HV [27–29].

MOBO experiment

The Initial data set consists of 18 experiments, selected by Latin Hypercube Sampling (LHS), ensuring a well-distributed initial exploration of the design space.

Given the time-intensive nature of process preparation, it is more practical to fabricate multiple samples in a single run rather than producing them sequentially. Therefore, batch selection was used for new sample evaluations instead of sequential selection. Each iteration of the optimization algorithm proposes a batch of 20 experiments, allowing the simultaneous fabrication and evaluation of samples with different input parameter values.

The acquisition function used in this study is Noisy Expected Hypervolume Improvement (qNEHVI), a state-of-the-art method for multi-objective Bayesian optimization. NEHVI is an extension of Expected Hypervolume Improvement (EHVI), designed to maximize the hypervolume of the Pareto front while accounting for uncertainty in noisy observations and discrete variable handling [30, 31].

3. Material characterisation

The quality of the obtained material, as a result of the laser melting process, was evaluated in terms of the obtained relative density. Grinded and polished 5x5mm xz plane cross sections of the sample were registered with the LEXT OLS4000 laser confocal microscope (Olympus, Tokio, Japan). To create a stitched image of the entire sample, 9 images were taken at magnification of x5. The registered images were analyzed with ImageJ v1.46r software, to quantify the total cross section ratio of the sample, which determined the porosity of the material.

The use of metallic materials with porosity higher than 5% in industrial applications is not justified, that is why the hardness of materials with porosity higher than 5% should not be measured because they do not meet the most important qualification criteria. However, to provide more data to evaluations, even if the measurements of highly porous samples are inaccurate, we also measured samples with porosity slightly higher than 5%.

Vickers hardness measurements were made using ZHVμ-A microhardness tester (Zwick-Roell, Leominster, United Kingdom). A load of 100 g was applied for 10 s to make a single indent and from each evaluated sample 12 indentations uniformly spaced on its area were taken. After the removal of two extreme measurements (the lowest and highest result), a mean hardness value of the sample and confidence levels were calculated.

4. Optimization steps

The optimization process consisted of 10 iterations and 20 samples each, proposed by the algorithm, which were fabricated and subsequently evaluated. This gives a total of 200 sample configurations. However, some of the suggested input parameter sets resulted in poor melting, preventing successful sample fabrication. Additionally, samples exhibiting excessively high porosity were excluded from hardness measurements, leading to a subset of processing conditions that were not fully evaluated. Therefore, some experiments conducted were unproductive and did not provide complete information to the optimization algorithm. Only samples that allow us to determine a complete set of information on all three evaluation criteria were considered as valid.

The primary objective of the optimization was to maximize the hypervolume indicator, a widely used metric in multi-objective optimization [32, 33]. Hypervolume quantifies the performance of the Pareto front by measuring the dominated volume in objective space, making it a robust criterion for assessing optimization progress. At each iteration, both the hypervolume and the corresponding Pareto front were plotted to visualize improvements in the optimization process and the evolution of trade-offs between competing objectives.

Results and discussion

The generated initial data set of experiments gives poor results in case of the number of valid samples. Only 11 of 18 were successfully built and evaluated in the case of porosity. Furthermore, only three of them gave satisfactory results that were reasonably to measure the material hardness. In total, only half of the suggested samples in the complete number of the optimization iterations were fully evaluated and provided satisfactory data for the optimization algorithm. Fig. 2 presents the effectiveness of subsequent sets of parameters suggested by the algorithm in the context of fabricable and measurable samples in terms of relative density, as well as those justified for measuring the hardness of the material. Besides this incomplete data provided from suggested experiments, evaluated algorithm quickly recognizes the processing window resulting in good melting and obtaining satisfactory results, and did not suggest more experiment sets with e.g. low laser energy, which failed to build the samples. In fact, from the total of 218 suggested experiment sets of 10 algorithm runs, only 95 manufactured samples were valid and provided complete data for modelled functions. The significant decrease in the number of built samples visible in the seventh iteration is due to the use of processing parameter values resulting in extremely high Build rate values (> 6mm^3/s) which, apart from this particular iteration, were suggested only in the initial set and in 1. Iteration.

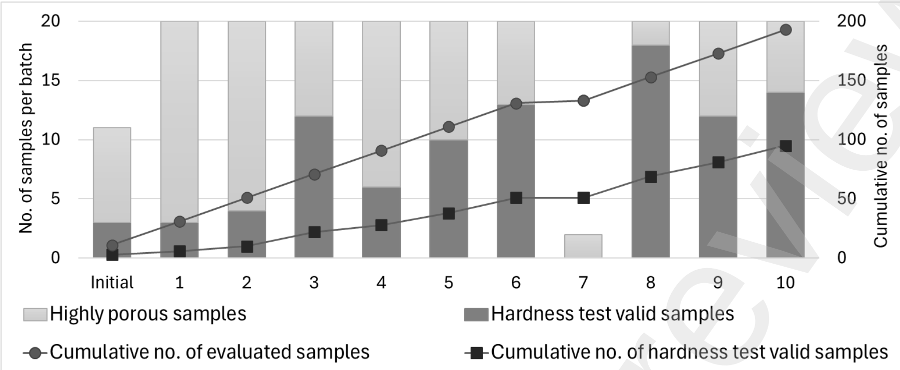

Fig. 2 The number of samples that were successfully produced in successive iterations of optimization, and that were assumed to exceed 95% relative density, could be subjected to hardness testing.

There are analytical ways to calculate the minimum energy density required to melt a material with defined characteristics, which could improve poor result in terms of number of valid samples, but each model has its limitations and does not take into account all the factors affecting melting. The aim of this study was to evaluate how BO algorithms can be useful in optimizing the process, treated as a 'black box' without detailed analytical preparation and without considering the physicochemical properties of the material being processed, which vary for each alloy and elemental composition.

The algorithm used in this study considers all samples that have a potentially 50% chance of being valid and searches within that design space. In addition, the optimization code can be modified for future research, to increase the likelihood of suggesting parameter sets that yield valid samples, with the option to apply this adjustment separately for each constraint.

The graphs in Fig. 3 show the location of points in the performance space discovered in the initial (a-c), 5th (d-f) and 10th (g-i) experiment iterations of the optimization. The design space covered by sample set in the initial experiment had good coverage, not only in case of the values of the input variables, but also in case of the obtained results, because samples with a relative density of 98.9% as well as in case of hardness close to targeted value were found (Fig. 3 a-c). Presented graphs (Fig. 3), alongside the quantities of fabricable and measurable samples in the context of the hardness (Fig. 2), shown that the more iterations of the experiment were carried out, the more effectively the algorithm searched the area of process parameter values resulting in high relative density and trying to increase the efficiency of the process.

The aim of the optimization was to maximize the obtained relative density (z_1) and build rate (z_2), while for z_3 – material hardness – to achieve a value as close as possible to 55 HV, which was achieved by minimizing the absolute value of the deviation of the measured value from the target hardness. For this reason, the points on the map of the distribution of the experiments carried out are convergent to the vertices of each system, and the hardness plots show the absolute value of the deviation and not the actual measured values for the samples.

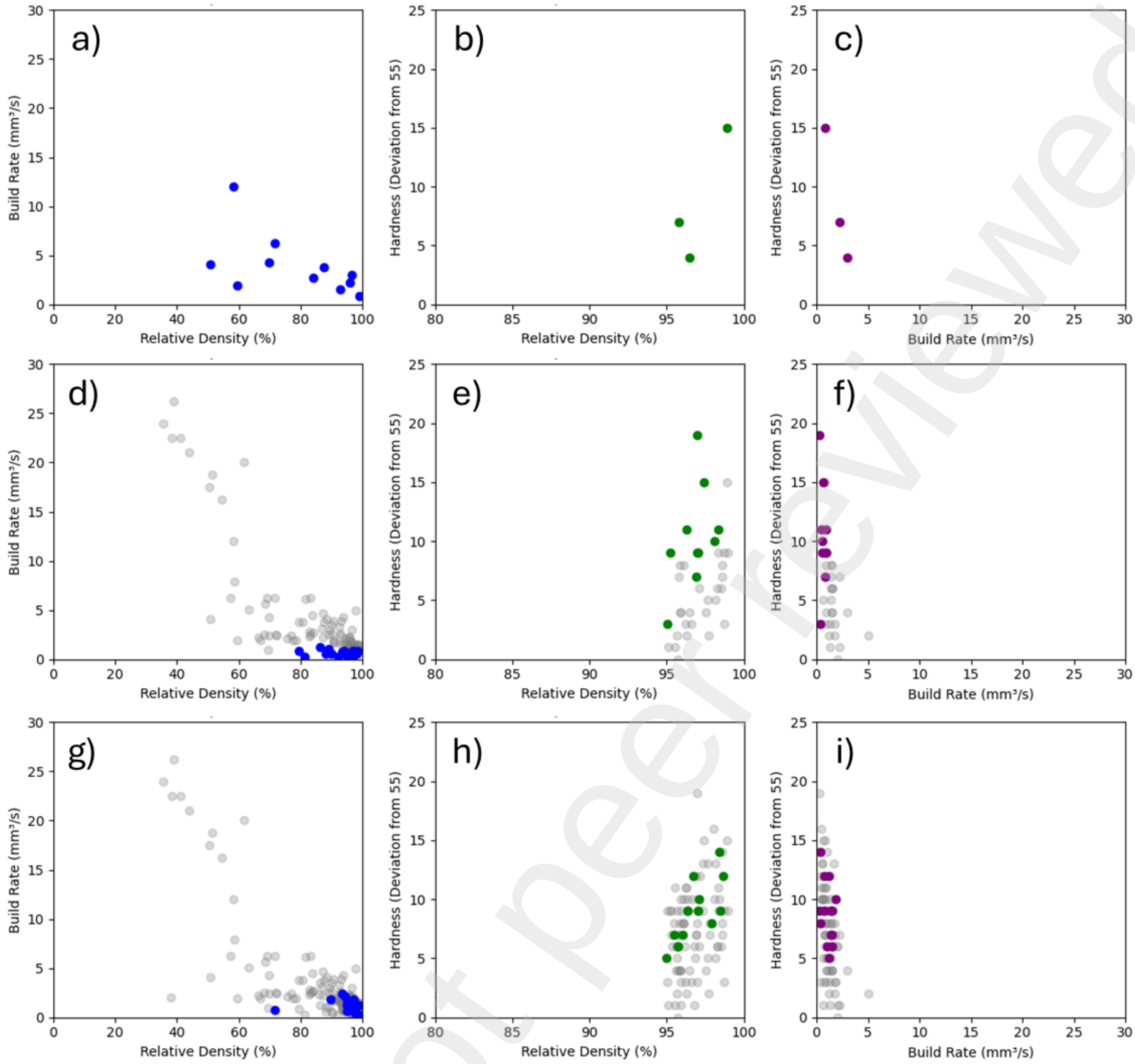

Fig. 3 Plots of the results of all measured samples tested in subsequent optimization runs: a-c - Initial data set, d-f - 5th optimization run, g-i - 10th optimization run; a, d, g - Relative density vs Build rate; b, e, h – Relative density vs. Hardness; c, f, i – Build rate vs. Hardness;

It should be noted that the real relative density evaluation measures were far from the predicted values, calculated based on approximation model built. The one reason for that could be the above-mentioned limited data used in optimization, that may have contributed to the poor alignment of the Gaussian process model, but the other is the fact that only one sample was evaluated for every input variable set. The PBF-LB/M process results, especially in a situation where there is high porosity in the samples, have low repeatability because of the process noise or other evaluation bias occurring. From our experience gained so far, the confidence levels for batches of samples built with the same processing conditions could vary even by 10 percentage points.

Analyzing the relationship between the obtained relative densities of the samples and process efficiency (Fig. 3 a, d, g) reveals a proportional trade-off: As process efficiency increases, material quality decreases. This confirms the mutual exclusivity of these two criteria and the inherent contradiction in the optimization process. For productivity values exceeding 5 mm³/s, achieving a relative density greater than 70% is not feasible. Conversely, parameter sets resulting in productivity below 5 mm³/s—particularly due to the wide range of laser power used, allow for the production of materials with a broad range of relative densities.

Of all samples measured after 10 optimization iterations, 15 points belonging to the Pareto front were identified. A set of all measured values and the values of the parameters used to derive them is summarized in Table 3, and are highlighted in red on the graphs in Fig. 4.

Table 3 The set of 15 experiments, belonging to the designated Pareto front.

Sample No.	Run	Laser Power [W]	Point distance [µm]	Exposure time [µs]	Hatch distance [µm]	Scanning velocity [mm/s]	VED [J/mm^3]	Relative density [%]	Build rate [mm^3/s]	Hardness [HV0.1]
3	Initial	100	150	500	150	300.0	44.44	95.76	2.25	62
12	Initial	100	70	200	50	350.0	114.29	98.88	0.88	70
13	Initial	75	80	160	120	500.0	25.00	96.46	3.00	51
62	03	100	150	180	120	833.3	20.00	97.74	5.00	57
63	03	70	90	460	150	195.7	47.70	98.59	1.47	63
64	03	100	50	360	150	138.9	96.00	98.69	1.04	64
67	03	85	60	160	80	375.0	56.67	98.55	1.50	61
78	03	100	60	500	150	120.0	111.11	98.95	0.90	64
100	05	50	50	480	50	104.2	192.00	96.96	0.26	74
137	06	100	120	460	150	260.9	51.11	96.76	1.96	61
169	08	55	60	360	60	166.7	110.00	98.01	0.50	71
174	08	75	60	180	60	333.3	75.00	98.58	1.00	69
180	09	90	50	180	120	277.8	54.00	98.13	1.67	68
203	10	100	60	180	110	333.3	54.55	97.11	1.83	65
207	10	65	50	280	140	178.6	52.00	98.65	1.25	67

On the other hand, for plotted points for deviations, the Pareto front cuts off the vertex of the performance space (Fig. 4).

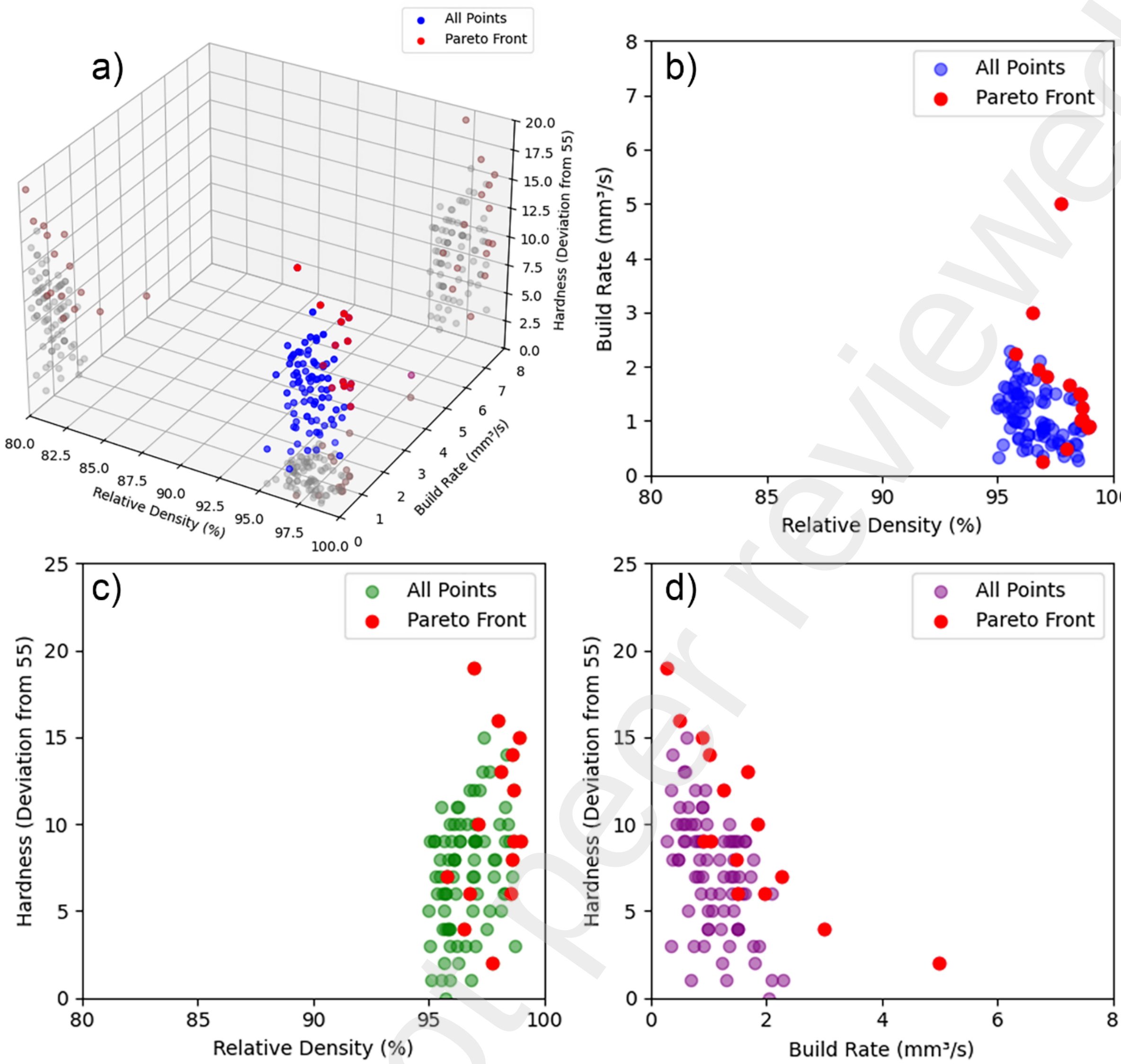

Fig. 4 The designated Pareto front after 10 experiment runs; a) 3D space with points projection to planar surfaces; b-d) 2D performance space plots with highlighted points from Pareto front

The hypervolume improvement across the consecutive experiments performed is presented in Fig. 5. To make the hypervolume plots for each iteration more comparable, the reference point used to calculate the values was constant. The evaluated optimization criteria for valid samples took values of 95.00-98.95, 0.26-5.00 and -4.0-19.0 respectively; therefore, the reference point coordinates were selected as -80.0, 0.0, 25.0.

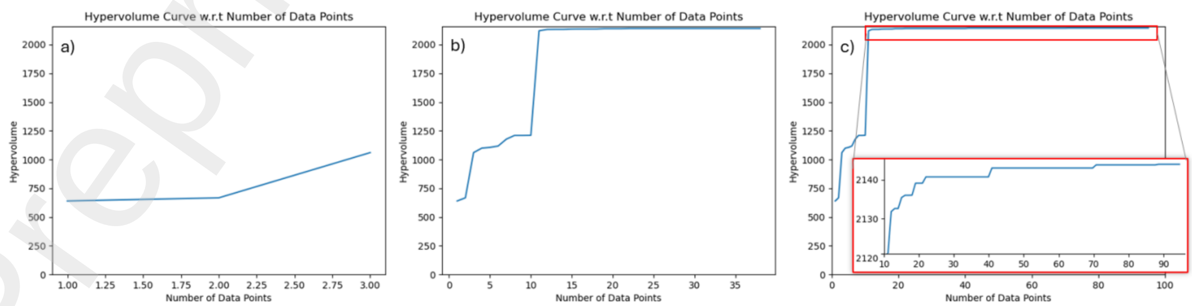

Fig. 5 Hypervolume improvement; a) initial data; b) after 5th experiment; c) after 10th experiment

At first glance, subsequent experiments after 20 evaluated valid samples (from 88 samples tested in total) do not bring hypervolume improvements, but if we look closely (Fig. 5c), we can see that each subsequent iteration leads to further slight increases in hypervolume value. The maximum value of 2154, was reached in 9^{th} optimization run.

The results of the optimization included in this study would not be complete if we did not present the quality of the obtained material in the selected samples. Fig. 6 shows microscopic images of selected samples belonging to the Pareto front in the context of defects (pores) in the material.

When analyzing microscopic images depending on the values of process parameters used, resulting in the build rate and relative density, a clear increase in pore size can be observed with an increase in the build rate. Although comparable relative density values were achieved between samples No. 62 and 169, the difference of 4.5 mm3/s in the build rate makes the melting of the material not as accurate. In the sample material made with a higher process build rate, there are many keyhole pores and loose spaces arranged in vertical pattern lines, suggesting a poor connection between the remelted hatching scans. On the other hand, samples produced with low process efficiencies (<2 mm^3/s) contain fine gas pores uniformly dispersed in the sample volume.

From the material strength point of view, both the size of the pores and their shape are crucial. Evenly dispersed, fine gas porosity does not have such a negative effect on strength impairment as uneven, large lack-of-fusion pores, and keyholes. Hot isostatic pressing (HIP) postprocess treatment can be an effective method of eliminating porosity in the material, even for large and irregular pores. Such studies will be carried out in the future to evaluate the healing effect in magnesium alloys using HIP.

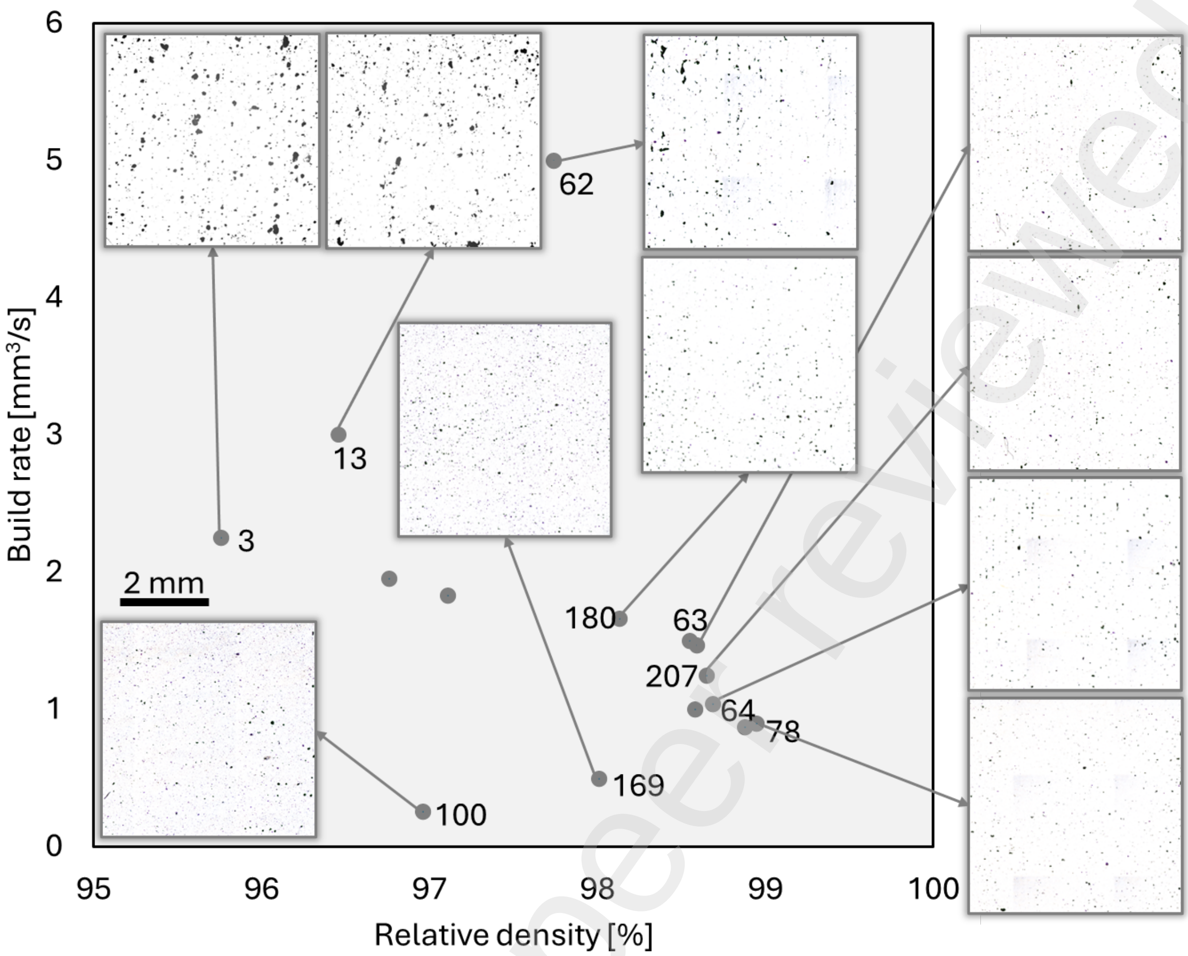

Fig. 6 Microscopic images of selected samples belonging to the Pareto front.

By relating the obtained results of relative density and the measured hardness to the previously quoted descriptive parameter of the PBF-LB/M process – Volume Energy Density (VED), a clear exponential relationship for the density of the material can be noticed (Fig 7). However, when recalling this trend, it is still necessary to keep in mind the phenomenon of evaporation of alloying elements along with the increase in temperature during remelting, along with the increase in VED. In addition, it is worth noting that even with an energy density of less than 50 J/mm^3, it is possible to obtain samples with a relative density of >95% (Fig. 7a).

The material hardness also increases with increasing VED (Fig. 7b). The change in the chemical composition of the material as a result of the evaporation of magnesium possibly causes an increase in the content of aluminium in the alloy. The hardness of pure magnesium is approximately 40 HV, while the hardness of pure aluminium is 50% higher and amounts to approximately 60 HV. Despite this, the hardness of all samples with a high relative density of the material is higher than the target 55 HV. This is the result of the grain refinement in the material microstructure – characteristic for the PBF-LB/M process which has a direct correlation with the material hardness.

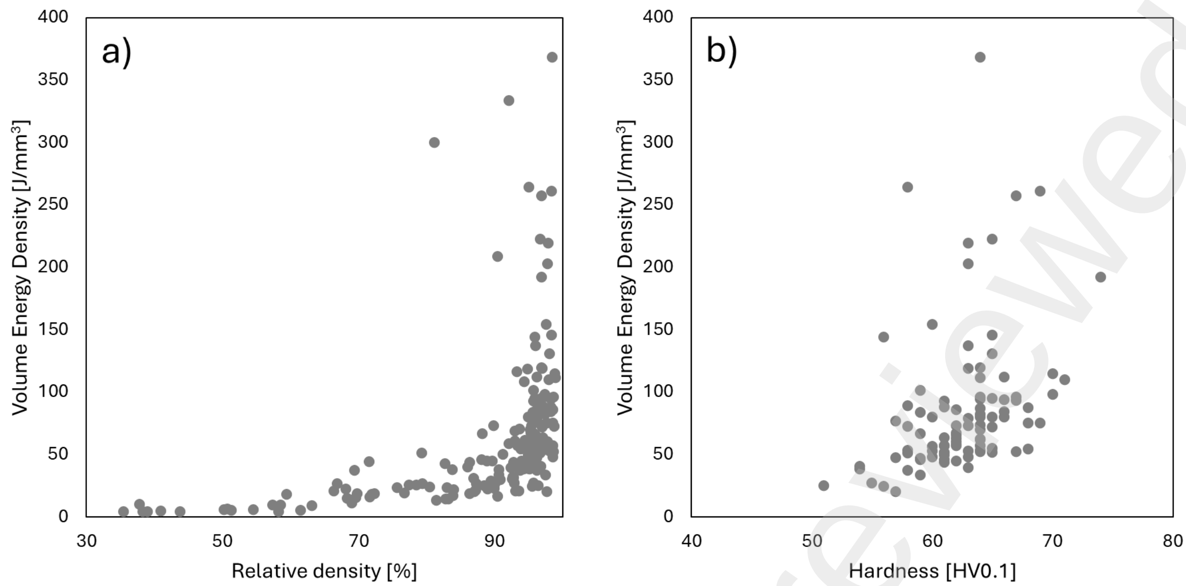

Fig. 7 The relation between applied Volume Energy Density (VED) and resulting material relative denisty (a) and absolute hardness (b).

Conclusion

This paper presents how effective the application of multi-criteria Bayesian optimization tools can be in process optimization, on the example of magnesium alloy processing in PBF-LB/M technology. The approach presented in this paper allows one to achieve a wide spectrum of results and information about the process and its results, in relation to the previously used approach using experimental plans [9]. In the cited work, for only three changed process parameters in a strongly narrowed range, it was necessary to examine more than 90 samples to determine the process window for only one criterion – relative density.

The use of multi-criteria optimization, with a comparable workload, removes the requirements for the initial limitation of the range of tested parameter values. In addition, the result is a process performance map for three evaluation criteria at the same time, which will allow you to focus further optimization on the selected goal.

In addition, instead of batch, a sequential method could be more efficient in the case of sample evaluation. Although batch sample printing is more time efficient, in the case of time savings in process preparation, images of not all samples could be necessary if they lead to results that did not improve the hypervolume indicator. If we would like to deal also with larger samples cross-sections, preparation of metallographic cross-sections will also take more time instead of polishing more samples at once. As a potential solution a hybrid optimization – suggesting subsequent samples to be produced in batches, and their sequential evaluation based on sample prioritization, would be more efficient. In this approach, the decision to select additional samples for measurements could be made based on the operator's own experience, but the algorithm could also point out which sample should be measured and which could be skipped. This can provide information to the modelled function about the explored design space more quickly, e.g., which samples do not bring the expected hypervolume improvement, saving time on the evaluation of samples from the vicinity of the studied design space.

The results presented in the paper show that this approach is particularly effective in process optimization. This tool is particularly helpful in process optimization for completely new materials, for which it is not yet possible to find literature reports that could be a starting point for narrowing down the values of the changed parameters.

Acknowledgments

A. Pawlak acknowledges the MIT-Poland Lockheed Martin Seed Fund for the opportunity initiation of such an interesting international collaboration between Massachusetts Institute of Technology and Wroclaw University of Science and Technology.

Funding

This work was supported by the National Science Centre Poland (NCN) [Narodowe Centrum Nauki] under the MINIATURA 8 programme (grant number 2024/08/X/ST8/00237).

Data availability statement

Source data will be made available in a publicly available repository after the publication of this work.
The source data will include Process-Structure-Property table with measured values for each set of parameters tested, tables with full hardness results for all 95 measured samples, as well as microscopic images of the cross-sections of the samples.

Code availability statement

The Python source code used in the optimization will be made available in an open repository (GitHub).

References

1. Pfaff, A., Jäcklein, M., Schlager, M., Harwick, W., Hoschke, K., Balle, F.: An Empirical Approach for the Development of Process Parameters for Laser Powder Bed Fusion. Materials 2020, Vol. 13, Page 5400. 13, 5400 (2020). https://doi.org/10.3390/MA13235400.

2. Xiong, W., Hao, L., Li, Y., Tang, D., Cui, Q., Feng, Z., Yan, C.: Effect of selective laser melting parameters on morphology, microstructure, densification and mechanical properties of supersaturated silver alloy. Mater Des. 170, 107697 (2019). https://doi.org/10.1016/J.MATDES.2019.107697.

3. Kosiba, K., King, W., Han, J., Paul, B., Kononenko, D.Y., Otto, M., Chernyavsky, D., van den Brink, J., Scudino, S., Hufenbach, J.K.: Fabrication of filigree parts via laser powder bed fusion: From melt spots to stents. Opt Laser Technol. 180, 111485 (2025). https://doi.org/10.1016/J.OPTLASTEC.2024.111485.

4. Wits, W.W., Bruins, R., Terpstra, L., Huls, R.A., Geijselaers, H.J.M.: Single scan vector prediction in selective laser melting. Addit Manuf. 9, 1–6 (2016). https://doi.org/10.1016/J.ADDMA.2015.12.001.

5. Scipioni Bertoli, U., Wolfer, A.J., Matthews, M.J., Delplanque, J.P.R., Schoenung, J.M.: On the limitations of Volumetric Energy Density as a design parameter for Selective Laser Melting. Mater Des. 113, 331–340 (2017). https://doi.org/10.1016/J.MATDES.2016.10.037.

6. Bosio, F., Aversa, A., Lorusso, M., Marola, S., Gianoglio, D., Battezzati, L., Fino, P., Manfredi, D., Lombardi, M.: A time-saving and cost-effective method to process alloys by Laser Powder Bed Fusion. Mater Des. 181, 107949 (2019). https://doi.org/10.1016/J.MATDES.2019.107949.

7. Gockel, J., Sheridan, L., Koerper, B., Whip, B.: The influence of additive manufacturing processing parameters on surface roughness and fatigue life. Int J Fatigue. 124, 380–388 (2019). https://doi.org/10.1016/J.IJFATIGUE.2019.03.025.

8. Sun, Z., Tan, X., Tor, S.B., Yeong, W.Y.: Selective laser melting of stainless steel 316L with low porosity and high build rates. Mater Des. 104, 197–204 (2016). https://doi.org/10.1016/J.MATDES.2016.05.035.

9. Pawlak, A., Rosienkiewicz, M., Chlebus, E.: Design of experiments approach in AZ31 powder selective laser melting process optimization. Archives of Civil and Mechanical Engineering. 17, 9–18 (2017). https://doi.org/10.1016/j.acme.2016.07.007.

10. Hoppe, V., Pawlak, A., Szymczyk-Ziółkowska, P., Jaśkiewicz, T., Rusińska, M., Dybała, B.: Investigation of Ti-13Nb-13Zr alloy powder properties and development of the L-PBF process. Mater Des. 217, 110546 (2022). https://doi.org/10.1016/j.matdes.2022.110546.

11. Li, B., Deng, B., Shou, W., Oh, T.H., Hu, Y., Luo, Y., Shi, L., Matusik, W.: Computational discovery of microstructured composites with optimal stiffness-toughness trade-offs. Sci Adv. 10, (2024). https://doi.org/10.1126/SCIADV.ADK4284/ASSET/380859A9-2B78-46C0-BBCB-6B2CACECF96F/ASSETS/IMAGES/LARGE/SCIADV.ADK4284-F4.JPG.

12. Liu, D., Wang, Y.: Metal Additive Manufacturing Process Design based on Physics Constrained Neural Networks and Multi-Objective Bayesian Optimization. Manuf Lett. 33, 817–827 (2022). https://doi.org/10.1016/J.MFGLET.2022.07.101.

13. Li, Z., Zhong, J., Jiang, X., Wang, Z., Zhang, L.: Accelerating lPBF process optimisation for NiTi shape memory alloys with enhanced and controllable properties through machine learning and multi-objective methods. Virtual Phys Prototyp. 19, (2024). https://doi.org/10.1080/17452759.2024.2364221.

14. Heddar, M.I.E., Mehdi, B., Matougui, N., Tahan, S.A., Jahazi, M.: Adaptable multi-objective optimization framework: application to metal additive manufacturing. International Journal of Advanced Manufacturing Technology. 132, 1897–1914 (2024). https://doi.org/10.1007/S00170-024-13489-9/FIGURES/1.

15. Saunders, R.N., Teferra, K., Elwany, A., Michopoulos, J.G., Lagoudas, D.: Metal AM process-structure-property relational linkages using Gaussian process surrogates. Addit Manuf. 62, 103398 (2023). https://doi.org/10.1016/J.ADDMA.2023.103398.

16. Chen, Y., Tian, Y., Zhou, Y., Fang, D., Ding, X., Sun, J., Xue, D.: Machine learning assisted multi-objective optimization for materials processing parameters: A case study in Mg alloy. J Alloys Compd. 844, 156159 (2020). https://doi.org/10.1016/J.JALLCOM.2020.156159.

17. Zhang, M., Sun, C.N., Zhang, X., Goh, P.C., Wei, J., Hardacre, D., Li, H.: High cycle fatigue life prediction of laser additive manufactured stainless steel: A machine learning approach. Int J Fatigue. 128, 105194 (2019). https://doi.org/10.1016/J.IJFATIGUE.2019.105194.

18. Chepiga, T., Zhilyaev, P., Ryabov, A., Simonov, A.P., Dubinin, O.N., Firsov, D.G., Kuzminova, Y.O., Evlashin, S.A.: Process Parameter Selection for Production of Stainless Steel 316L Using Efficient Multi-Objective Bayesian Optimization Algorithm. Materials 2023, Vol. 16, Page 1050. 16, 1050 (2023). https://doi.org/10.3390/MA16031050.

19. Song, B.U., Joon, ·, Choi, P., Lee, P.-H., Jung, M.-K., Shin, D., Ha, T., Lee, I.: Efficient Optimization of Magnetic Properties of Fe–4.5Si Alloy in Laser Powder Bed Fusion (LPBF). International Journal of Precision Engineering and Manufacturing-Green Technology 2025. 1–14 (2025). https://doi.org/10.1007/S40684-024-00683-Z.

20. Khalil, M., Teichert, G.H., Alleman, C., Heckman, N.M., Jones, R.E., Garikipati, K., Boyce, B.L.: Modeling strength and failure variability due to porosity in additively manufactured metals. Comput Methods Appl Mech Eng. 373, 113471 (2021). https://doi.org/10.1016/J.CMA.2020.113471.

21. Zhang, J., Yin, C., Xu, Y., Sing, S.L.: Machine learning applications for quality improvement in laser powder bed fusion: A state-of-the-art review. International Journal of AI for Materials and Design. 1, 26 (2024). https://doi.org/10.36922/ijamd.2301.

22. Sousa, J., Sousa, A., Brueckner, F., Reis, L.P., Reis, A.: Human-in-the-loop Multi-objective Bayesian Optimization for Directed Energy Deposition with in-situ monitoring. Robot Comput Integr Manuf. 92, 102892 (2025). https://doi.org/10.1016/J.RCIM.2024.102892.

23. Liu, J., Ye, J., Silva Izquierdo, D., Vinel, A., Shamsaei, N., Shao, S.: A review of machine learning techniques for process and performance optimization in laser beam powder bed fusion additive manufacturing. J Intell Manuf. 34, 3249–3275 (2023). https://doi.org/10.1007/S10845-022-02012-0/FIGURES/11.

24. Kurzynowski, T.: Metoda projektowania implementacji technologii selektywnej laserowej Mikrometalurgii proszków. Oficyna Wydawnicza Politechniki Wrocławskiej, Wrocław (2019).

25. Herzog, D., Bartsch, K., Bossen, B.: Productivity optimization of laser powder bed fusion by hot isostatic pressing. Addit Manuf. 36, 101494 (2020). https://doi.org/10.1016/j.addma.2020.101494.

26. Wang, W., van Keulen, F., Wu, J.: Fabrication sequence optimization for minimizing distortion in multi-axis additive manufacturing. Comput Methods Appl Mech Eng. 406, 115899 (2023). https://doi.org/10.1016/J.CMA.2023.115899.

27. Kim, J.Y., Hwang, J.W., Lee, S.M., Hyun, C.Y., Park, I.K., Byeon, J.W.: Effect of process variables on friction stirred microstructure and surface hardness of AZ31 magnesium alloy. Archives of Metallurgy and Materials. 64, 907–911 (2019). https://doi.org/10.24425/AMM.2019.129470.

28. Rashad, M., Pan, F., Liu, Y., Chen, X., Lin, H., Pan, R., Asif, M., She, J.: High temperature formability of graphene nanoplatelets-AZ31 composites fabricated by stir-casting method. Journal of Magnesium and Alloys. 4, 270–277 (2016). https://doi.org/10.1016/J.JMA.2016.11.003.

29. Sun, S., Deng, N., Zhang, H., He, L., Zhou, H., Han, B., Gao, K., Wang, X.: Microstructure and mechanical properties of AZ31 magnesium alloy reinforced with novel sub-micron vanadium particles by powder metallurgy. Journal of Materials

Research and Technology. 15, 1789–1800 (2021). https://doi.org/10.1016/J.JMRT.2021.09.015.

30. Daulton, S., Balandat, M., Bakshy, E.: Differentiable Expected Hypervolume Improvement for Parallel Multi-Objective Bayesian Optimization. In: Advances in Neural Information Processing Systems 33 (NeurIPS 2020). pp. 9851–9864 (2020).

31. Daulton, S., Balandat, M., Bakshy, E.: Parallel Bayesian Optimization of Multiple Noisy Objectives with Expected Hypervolume Improvement. In: Advances in Neural Information Processing Systems 34 (NeurIPS 2021). pp. 2187–2200 (2021).

32. Audet, C., Bigeon, J., Cartier, D., Le Digabel, S., Salomon, L.: Performance indicators in multiobjective optimization. Eur J Oper Res. 292, 397–422 (2021). https://doi.org/10.1016/J.EJOR.2020.11.016.

33. Riquelme, N., Von Lücken, C., Barán, B.: Performance metrics in multi-objective optimization. Proceedings - 2015 41st Latin American Computing Conference, CLEI 2015. (2015). https://doi.org/10.1109/CLEI.2015.7360024.

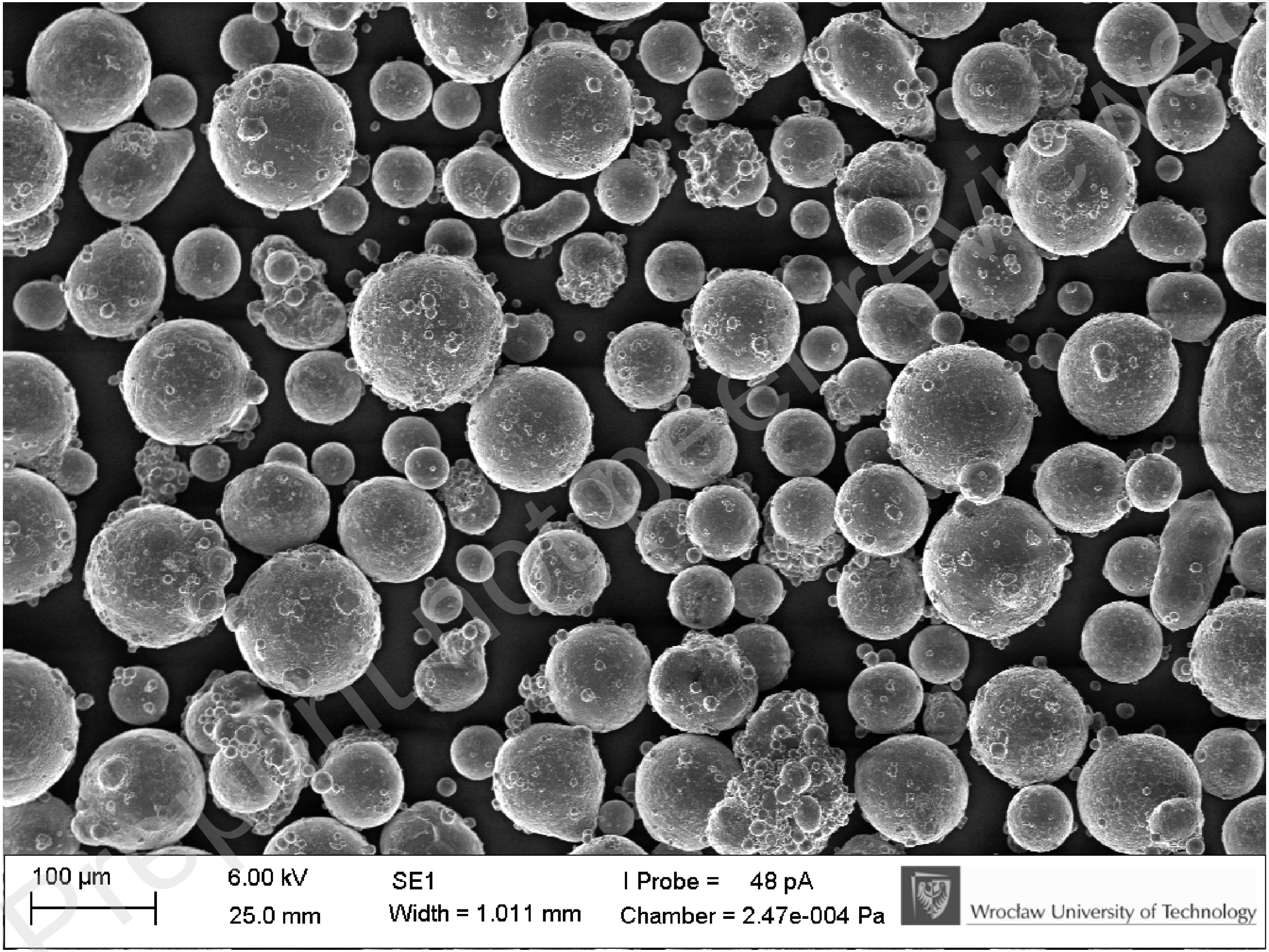
100 µm
6.00 kV
25.0 mm
SE1
Width = 1.011 mm
I Probe = 48 pA
Chamber = 2.47e-004 Pa
Wrocław University of Technology

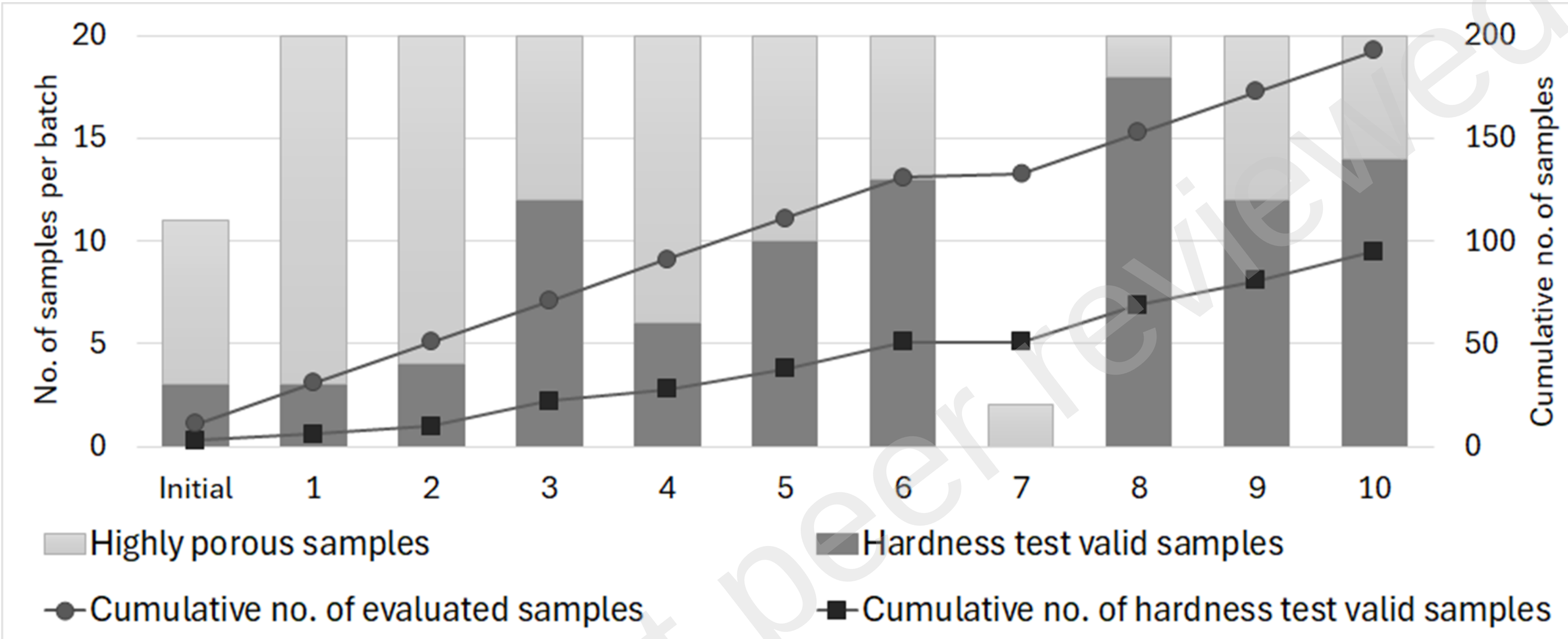

No. of samples per batch
Cumulative no. of samples
20
15
10
5
0
200
150
100
50
0
Initial
1
2
3
4
5
6
7
8
9
10
Highly porous samples
Hardness test valid samples
Cumulative no. of evaluated samples
Cumulative no. of hardness test valid samples

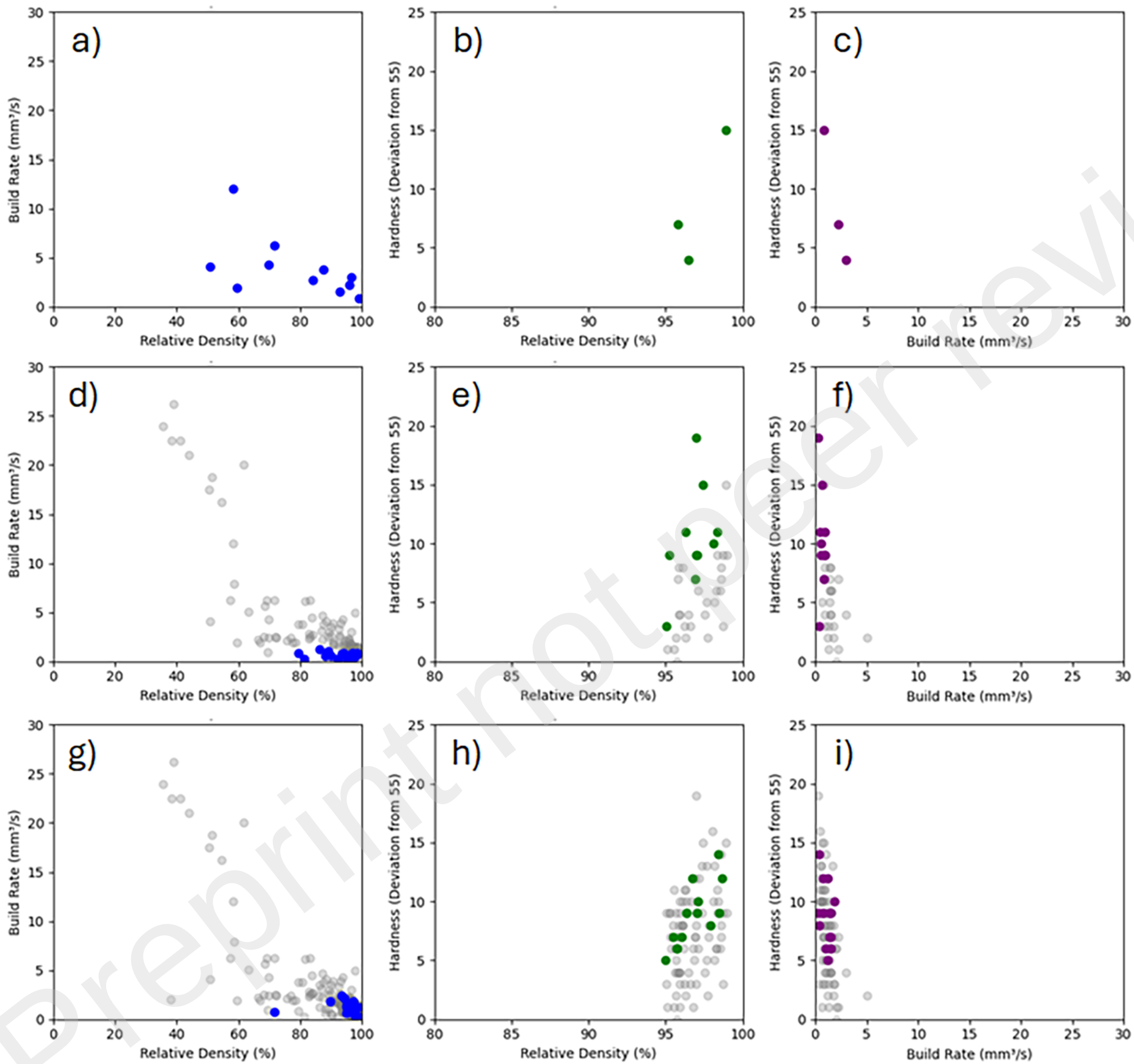
a)
b)
c)
d)
e)
f)
g)
h)
i)
Build Rate (mm³/s)
Relative Density (%)
Hardness (Deviation from 55)
Build Rate (mm³/s)

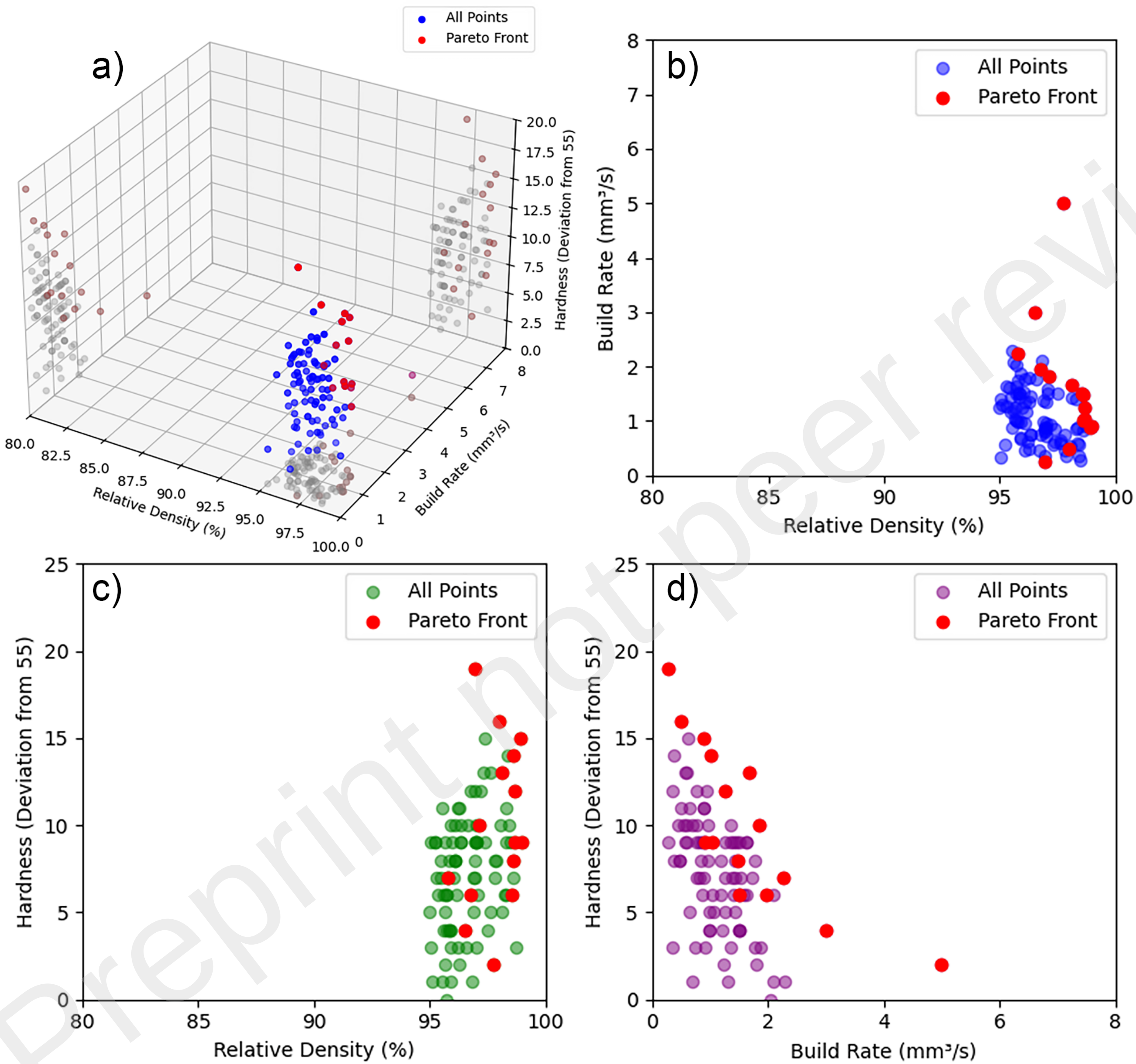

a)
All Points
Pareto Front
Relative Density (%)
Build Rate (mm³/s)
Hardness (Deviation from 55)
b)
All Points
Pareto Front
Build Rate (mm³/s)
Relative Density (%)
c)
All Points
Pareto Front
Hardness (Deviation from 55)
Relative Density (%)
d)
All Points
Pareto Front
Hardness (Deviation from 55)
Build Rate (mm³/s)

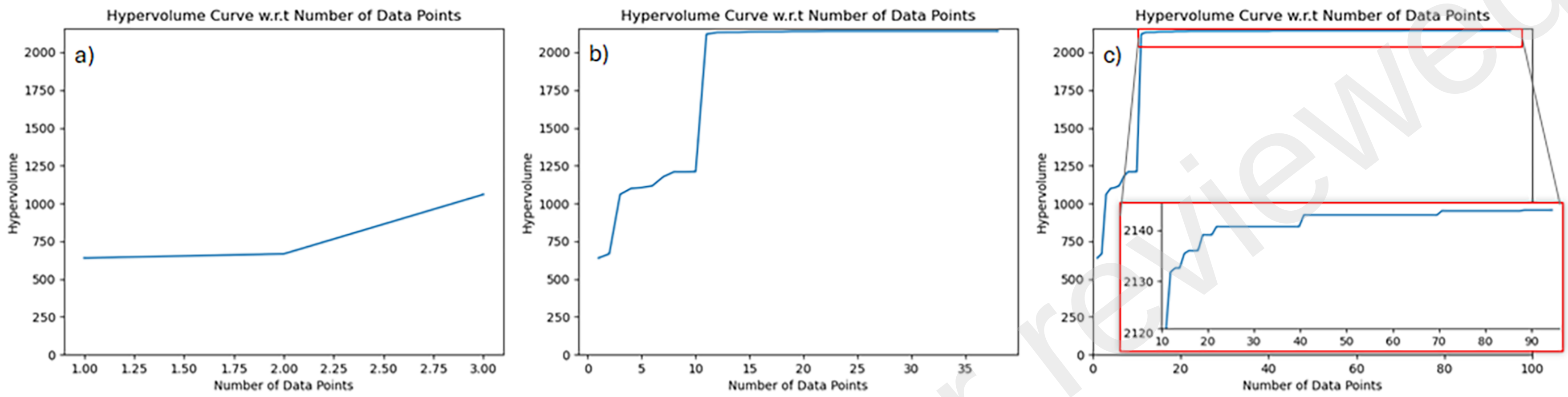
Hypervolume Curve w.r.t Number of Data Points
a)
b)
c)
Hypervolume
Number of Data Points

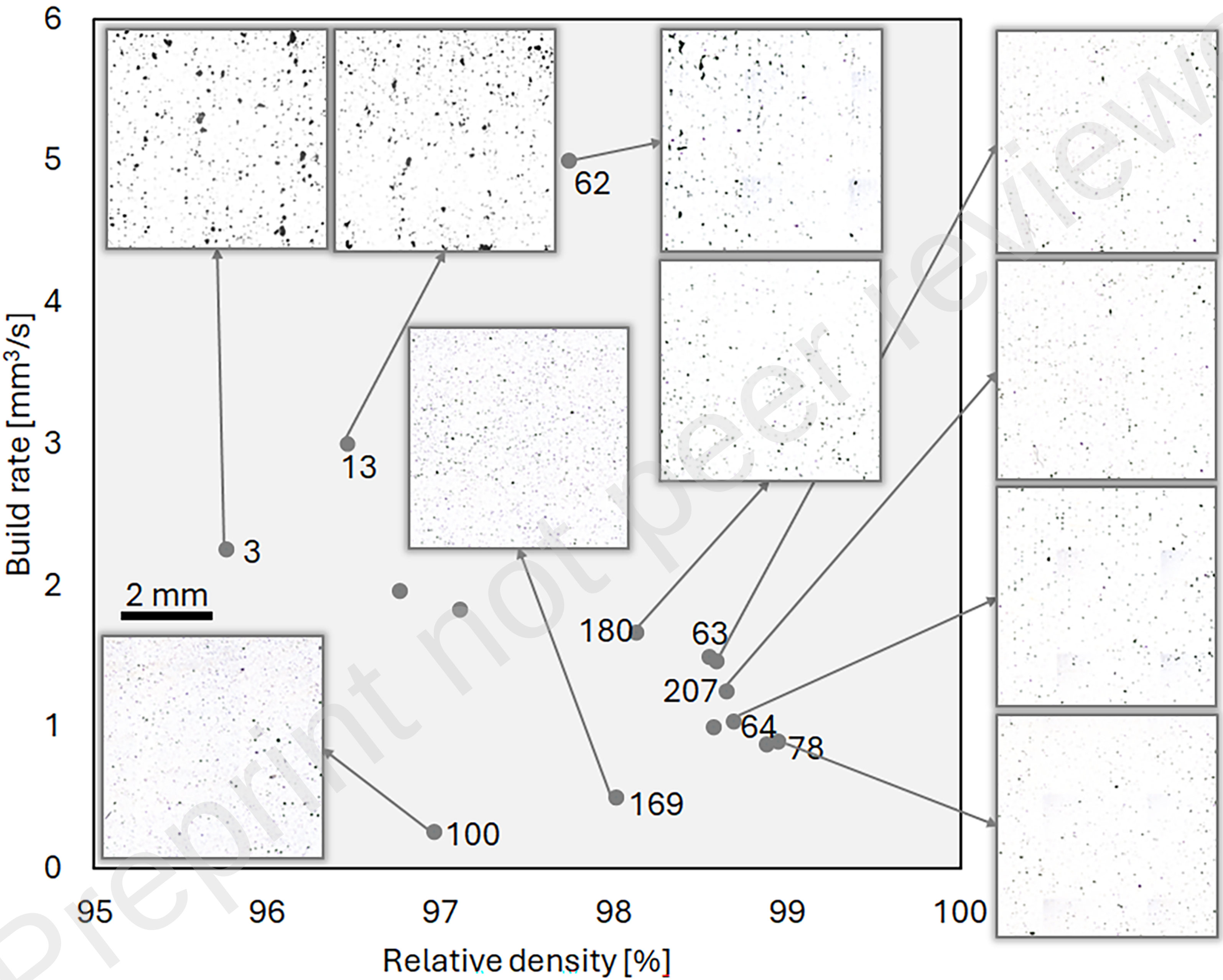

Build rate [mm³/s]
Relative density [%]
0
1
2
3
4
5
6
95
96
97
98
99
100
2 mm
3
13
62
100
169
180
63
207
64
78

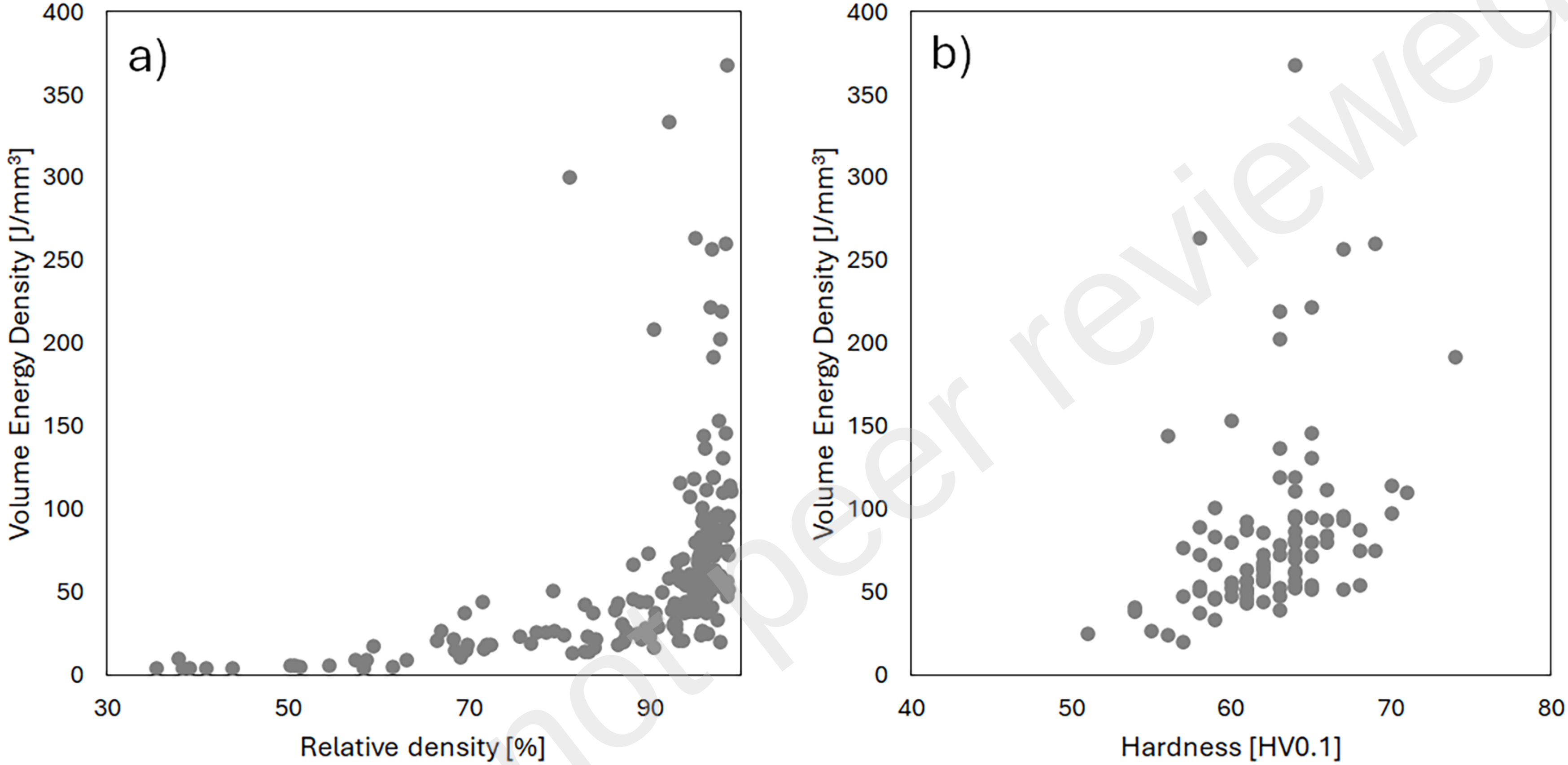
a)
b)
Volume Energy Density [J/mm³]
Relative density [%]
Hardness [HV0.1]
400
350
300
250
200
150
100
50
0
30
50
70
90
40
60
80

Table 1 The list of input variables, their possible values ranges, limited to the scope studied in this paper, and the size of the value change step.

Process Parameter		**Available range**	**Range**	**Step size**
P	Laser power [W]	0.02-100	5-100	5 W
p_{dist}	Distance between scanning points [μm]	1-1000	50-150	10 μm
t_{expo}	Laser exposure time [μs]	20-1000	20-500	20 μs
h_{dist}	Distance between scanned tracks [μm]	1-1000	50-150	10 μm

Table 1 The List of criteria for evaluating the effects of the process and their goal in optimization.

Optimization criteria		Max/min
z_1	Relative density [%]	Maximize
z_2	Build rate [mm^3/s]	Maximize
z_3	Hardness [HV0.1]	Minimize deviation from 55

Table 1 The set of 15 experiments, belonging to the designated Pareto front.

Sample No.	Run	Laser Power [W]	Point distance [µm]	Exposure time [µs]	Hatch distance [µm]	Scanning velocity [mm/s]	VED [J/mm^3]	Relative density [%]	Build rate [mm^3/s]	Hardness [HV0.1]
3	Initial	100	150	500	150	300.0	44.44	95.76	2.25	62
12	Initial	100	70	200	50	350.0	114.29	98.88	0.88	70
13	Initial	75	80	160	120	500.0	25.00	96.46	3.00	51
62	03	100	150	180	120	833.3	20.00	97.74	5.00	57
63	03	70	90	460	150	195.7	47.70	98.59	1.47	63
64	03	100	50	360	150	138.9	96.00	98.69	1.04	64
67	03	85	60	160	80	375.0	56.67	98.55	1.50	61
78	03	100	60	500	150	120.0	111.11	98.95	0.90	64
100	05	50	50	480	50	104.2	192.00	96.96	0.26	74
137	06	100	120	460	150	260.9	51.11	96.76	1.96	61
169	08	55	60	360	60	166.7	110.00	98.01	0.50	71
174	08	75	60	180	60	333.3	75.00	98.58	1.00	69
180	09	90	50	180	120	277.8	54.00	98.13	1.67	68
203	10	100	60	180	110	333.3	54.55	97.11	1.83	65
207	10	65	50	280	140	178.6	52.00	98.65	1.25	67